Author Manuscript

Author Manuscript

Author Manuscript

Author Manuscript

HHS Public Access

Author manuscript

Nanoscale. Author manuscript; available in PMC 2015 March 11.

Published in final edited form as:

Nanoscale. 2013 November 7; 5(21): 10127–10140. doi:10.1039/c3nr03633b.

Plasmonic Nanoprobes: From Chemical Sensing to Medical Diagnostics and Therapy

Tuan Vo-Dinh[*], **Andrew Fales**, **Guy D. Griffin**, **Christopher Khoury**, **Yang Liu**, **Hoan Ngo**, **Stephen J. Norton**, **Janna Register**, **Hsin-Neng Wang**, and **Hsiangkuo Yuan**

Department of Biomedical Engineering, Department of Chemistry, and the Fitzpatrick Institute for Photonics, Duke University, Durham, NC 27708, USA

1) Introduction

The development of plasmonics-active nanosystems has received increasing interest for use in a wide variety of applications ranging from molecular manufacturing, environmental monitoring and chemical sensing to medical diagnostics and therapy. Plasmonics refers to the study and application of enhanced electromagnetic properties of metallic nanostructures. The term has its origin in the word “plasmon”, the quanta associated with longitudinal waves propagating in matter through the collective motion of large numbers of electrons. According to classical electromagnetic theory, when a metallic nanostructured surface is irradiated by an incident electromagnetic field (e.g., a laser beam), conduction electrons are displaced into frequency oscillations equal to those of the incident light. These oscillating electrons, referred to as “surface plasmons,” produce a secondary electric field, which adds to the incident field. Plasmon resonances of metallic nanoparticles are referred to as localized surface plasmons (LSPs). LSPs can be excited when light is incident on metallic nanoparticles whose size is much smaller than the wavelength of the incident light. Resonant dipolar and multipolar modes can be excited in the nanoparticles at specific spectral frequencies, inducing significant increase in absorbed and scattered light and enhancement of electromagnetic fields inside and near the particles. LSPs produce resonance peaks in the absorption or scattering spectra of the metallic nanoparticles. This condition yields intense localized fields, which can interact with molecules in contact with or near the metal surface. In an effect analogous to a “lightning rod”, secondary fields can become concentrated at points of high curvature on the nanostructured metal surface. Nanoparticles of noble metals such as gold and silver resonantly scatter and absorb light in the visible and near-infrared spectral region upon excitation of their plasmon oscillations, and are therefore materials of choice for plasmon-related devices. Surface plasmons have been associated with important practical applications in surface plasmon resonance (SPR), surface-enhanced Raman scattering (SERS) and surface-enhanced luminescence (also referred to as metal-enhanced luminescence).

Discovery of the SERS effect in the 1970s [1, 2] indicated that Raman scattering efficiency could be enhanced by factors of up to 10^6 when the sample is located on or near nano-

[*] Corresponding author: tuan.vodinh@duke.edu.

Author Manuscript Author Manuscript Author Manuscript Author Manuscript

textured surfaces of plasmonics-active metals such as silver, gold, and transition metals. These discoveries spurred great interest in the research and development of SERS as a general spectroscopic tool throughout the following decade [3-8]. However, this initial enthusiasm for SERS declined from the mid-1970s to the early 1980s due to the irreproducibility of preparing metal nanoparticles in colloidal solution. Furthermore, an additional limitation in the early development of SERS-based analytical methods was that SERS enhancement of Raman scattering had been observed for only a few highly polarizable small molecules, such as pyridine, benzoic acid and their derivatives. Most studies involved samples at concentrations between 10^{-1} and 10^{-3} M, which are well above the useful concentration ranges for trace analysis. As a result, the SERS effect found very few practical applications prior to the mid-1980s.

In 1984, we first reported the general applicability of SERS as an analytical technique, and demonstrated that the SERS phenomenon is in fact a general effect, and that it can be applied to a wide variety of chemicals including homocyclic and heterocyclic polyaromatic compounds [9]. We introduced the use of metal-coated nanostructures as efficient and reproducible plasmonics-active media, which has led to a wide variety of SERS platforms for chemical sensing [10-19], bioanalysis and biosensing [20-27], chemical analysis, medical diagnostics and therapy [28-61]. These nanoplatforms have involved microplates [9], optical fibers having silver-coated dielectric nanoparticles [22], nanorods [12], nanodots [54], and nanowires [55]. The fabrication process involves depositing a thin metal film on substrates having polystyrene nanospheres [9, 11-14, 42, 50], titanium dioxide [18], alumina [19], or on optical nanofibers [22]. More recently, unique structures such as gold nanostars have been developed as plasmonics-active probes for SERS detection [40, 41]. Figure 1 shows some examples of plasmonics SERS platforms that have been developed in our laboratory for SERS applications. These nanoplatforms have led to a myriad of applications including sensitive detection of chemicals with both environmental and biochemical significance [9, 21], chemical dyes in art works [31], organophosphorus and chlorinated toxicants, [15, 16], and DNA-adducts [13]. The SERS technique was first introduced as a new gene detection modality for a DNA hybridization assay in 1994 [20]. This research has led to further development of the SERS method for detecting biomarkers of disease such as DNA/RNA [30, 33, 34, 35, 44, 47, 49, 50] as well as medical theranostics (i.e., both diagnostics and therapeutics) applications [39, 40, 41, 46, 48, 51]. Certain mechanisms related to the SERS effect, such as the contribution of electromagnetic interactions, have been extensively investigated and are reasonably well understood. Moreover, it has been reported that SERS enhancement from the interstitial space (“hot spots”) between two or more nanoparticles can approach 10^{14} to 10^{15}, and allow single-molecule detection [62-64]. Theoretical calculations indicate that the maximum enhancement factor contributed by electromagnetic processes from “hot spots” is on the order of 10^{11}. Other enhancement processes such as the contribution of chemical effects are likely to induce further enhancement effects [65]. The SERS-based plasmonic technology is now receiving increased interest and contribution from many research groups worldwide.

This article provides an overview of the recent development and applications of plasmonic nanoprobes and nanosystems in our laboratory for the last few years. Various applications will be presented to illustrate the usefulness and potential of these nanoplatforms for

Author Manuscript Author Manuscript Author Manuscript Author Manuscript

chemical sensing and medical theranostics. The potential for combining the spectral selectivity and high sensitivity of the SERS process with the inherent molecular specificity of SERS plasmonic nanoprobes is discussed in the context of early diagnostics at the molecular level and providing a new tool set for the medicine of the future.

2) Label-Free 'Molecular Sentinel (MS)' Biosensing in Solution and on Nanochip *MS Homogeneous Assay in Solution*

A unique label-free detection method, called "Molecular Sentinel" (MS) incorporates the "SERS effect modulation" scheme associated with metallic nanoparticles and the DNA stem-loop structure [30]. Other research groups have investigated various nanoparticle-DNA systems and reported methods for quantitative DNA detection [66, 67] and gold nanoshell-mediated delivery and laser-triggered release of antisense oligonucleotide for gene silencing [68]. The plasmonics-based MS nanoprobe is composed of a SERS-active metal nanoparticle and a stem-loop DNA molecule tagged with a Raman label (Fig. 2A). The nanoprobe utilizes the specificity and selectivity of the DNA base sequence on the loop portion of the stem-loop probe to detect a specific target DNA sequence of interest by complementary base pair recognition and hybridization. In the normal configuration and in the absence of target DNA, the stem-loop configuration keeps the Raman label close to the metal nanoparticle, inducing an intense SERS effect that produces a strong Raman signal upon laser excitation (Fig 2B). Upon hybridization of a complementary target DNA sequence to the nanoprobe, the stem-loop configuration is disrupted, causing the Raman label to physically separate from the metal nanoparticle, thus quenching the SERS signal (Fig. 2C).

The operating principle of the detection strategy for the MS probes is based upon the change of the plasmonic strength of the SERS signal as a function of the distance between the metallic nanoparticle and the Raman label. The plasmonic enhancement is due to electromagnetic effects and chemical effects at the metal surface. Studies of electromagnetic effects have shown that the SERS enhancement, G factor, decreases as $G = [r/(r+d)]^{12}$ for a single analyte molecule located a distance d from the surface of a metal particle of radius r. The electromagnetic SERS enhancement falls off drastically with increasing distance between the label and the metallic nanoparticle due to the decay in the dipole over the distance $(1/d)^3$ to the fourth power, thus resulting in a total intensity decay of $(1/d)^{12}$. Because the Raman enhancement field decreases very significantly as a function of small dislocation from the surface, a molecule must be located very close (0–10 nm) to the nanoparticle surface in order to experience the enhanced local field. In the absence of target genes, the stem-loop configuration keeps the Raman label in contact or close proximity (< 1 nm) to the nanoparticle, thus inducing strong plasmonic enhancement and a strong SERS signal from the label (Fig. 2B). However, when complementary target DNA is recognized and captured (i.e., hybridized) by the MS nanoprobe, the SERS signal of the labels is drastically decreased, indicating target recognition and binding (Fig. 2C).

The SERS MS concept is a label-free technique because the target molecules do not have to be labeled. The technique is also appropriate for detecting the presence of specific DNA sequences in a homogenous solution. The SERS MS nanoprobe has been used to detect the

Author Manuscript Author Manuscript Author Manuscript Author Manuscript

presence of DNA sequences of the HIV gene [30], breast cancer genes [33] and single-nucleotide polymorphism [34]. The feasibility of multiplex DNA detection using the SERS-MS technique has also been demonstrated in a homogenous solution [33]. In this study two MS nanoprobes, ERBB2-MS and KI-67-MS, were designed and separately prepared to target breast cancer biomarkers, *erbB-2* and *ki-67* genes, respectively. These results demonstrate that the MS nanoprobe technique can provide a useful tool for multiplex DNA detection in a homogeneous solution for medical diagnostics and high-throughput bioassays. In addition, SERS measurements are performed immediately following the hybridization reactions without washing steps, which greatly simplifies the assay procedures. The results underline the advantage of the SERS-based MS nanoprobes over fluorescence-based assays for multiplex detection [33].

Molecular Sentinel on Chip

The label-free Molecular Sentinel biosensing concept was further developed and adapted for use on substrate platforms [44, 50]. A unique platform that is simple, inexpensive to fabricate is the Nanowave Chip [50]. The substrate, which consists of a metal film over closely packed nanospheres, was referred to as a “Nanowave” due to its resemblance to a periodic waveform, was first introduced in 1984 and used as a SERS-active substrate for the sensitive and reproducible detection of analytes [9]. The Nanowave platform, also referred to as metal film on nanopheres (MFON) and later used by other researchers [69], belongs to a subset of SERS-active substrates involving metal film coated on various nanoparticles, such as titanium dioxide [18] and alumina [19]. Numerical simulations were used to mimic the Nanowave geometry in three-dimensional space and to confirm its experimentally observed plasmonic behavior [42]. The study confirms that an in-plane polarized incident plane wave generates strong enhancements in the interstitial spaces between individual metal-coated nanospheres, thus producing closely packed arrays of hot spots which produce the strong SERS effect of the Nanowave substrate structures. The Nanowave chip fabrication was further refined to become simple with low-cost and high reproducibility using deposition of a thin shell of metal (e.g., gold) over closely packed arrays of nanospheres [50]. Use of a self-assembly on a water-air interface method can produce a large area of closed-packed nanosphere arrays for the Nanowave chip (Fig. 2D). The Nanowave chip fabrication is relatively simple and low-cost with high reproducibility. The sensing process involves a single hybridization step between the DNA target sequence and the complementary MS probes on the Nanowave chip without requiring secondary hybridization or post-hybridization washing, thus resulting in shorter assay time and less reagent usage (Fig. 2E). The usefulness and potential application of the biosensor for medical diagnostics is demonstrated by detecting the human RSAD2 (Viperin) gene, a common host biomarker of inflammation [50]. This gene is expressed as a response of the host immune system to the infection of various viruses such as the human cytomegalovirus (HCMV), influenza virus, hepatitis C virus (HCV), and retroviruses.

Author Manuscript Author Manuscript Author Manuscript Author Manuscript

3) Plasmonic Coupling Interference (PCI) Nanoprobes for Nucleic Acid Detection

In addition to the surface plasmon-induced enhanced electromagnetic (EM) fields within the region near the surface of metal nanoparticles, the EM field is particularly strong in the interstitial space where two adjacent nanospheres are in contact (often referred to as the “hot spot” region) [70]. Furthermore, the coupling of plasmonic structures could also produce hybridized plasmon modes leading to coherent phenomena based on coupled-oscillator processes, such as Fano resonances in coupled nanodisks [71]. The phenomenon involving the plasmonic coupling effect could also provide a further enhancement effect for SERS detection [52, 53]. The plasmonic coupling effect is due to the mutual enhancement of surface plasmon local electric fields of several nanoparticles that determine the dipole moment of a molecule trapped in a gap between particles. The magnitude of the EM field in the gaps depends on the separation distance between nanoparticles [36]. To practically control the separation distance between particles, DNA oligonucleotides have been utilized to assemble nanoparticles into an aggregate in a controllable manner.[72, 73] This self-assembly strategy has led to the development of sensitive DNA detection methods based on the plasmonic coupling effect.[74, 75]

We have developed a label-free, SERS-based DNA/RNA detection scheme called plasmonic coupling interference (PCI) [47], which combines the plasmonic coupling effect with DNA hybridization biosensing. Figure 3 schematically illustrates the basis of the PCI detection strategy. In this approach, oligonucleotide-functionalized nanoparticles are prepared as capture probes (Capture-NPs) and complementary Raman-labeled reporter probes (Reporter-NPs) (Figure 3A) are prepared and allowed to react in order to assemble nanoparticles into nano-aggregates. To induce the plasmonic coupling effect, Capture-NPs and Reporter-NPs are mixed in a hybridization buffer solution in order to form nano-aggregates mediated by capture/reporter oligonucleotide duplexes having the Raman label located between adjacent NPs (Figure 3B). In this situation the Raman label molecules located between two nanoparticles (hot spot area) experience a strong plasmonic coupling effect, which induces an intense SERS signal of the Raman labels upon laser excitation. When the target sequences are introduced to the sample, they will act as competitors of the Reporter-NPs in a competitive binding process. As a result, the plasmonic coupling is interfered with by the target molecules and the SERS signal is significantly reduced (Fig. 3C).

The PCI technique was used for the detection of microRNA sequences, which are a class of small noncoding endogenous RNA molecules emerging as promising biomarkers for cancer diagnostics and classification. For proof of concept, the miR-21 microRNA was used as a model since it has been identified as an oncogene overexpressed in a variety of different tumors. We designed the unlabeled capture probe and the Cy3-labeled reporter probe with the sequences of 5’-SHTCAACATCAGTCTGATAAGCTA-3’ and 5’-SH-TAGCTTATCAGAC-Cy3-3’, respectively, for the detection of the mature human microRNA miR-21 molecule with the sequence of 5’-UAGCUUAUCAGACUGAUGUUGA-3’. The unlabeled capture-(miR21)-probes are fully complementary to the mature miR-21 sequences and the Cy3-labeled reporter-(miR21)-

Author Manuscript Author Manuscript Author Manuscript Author Manuscript

probes are complementary to a partial sequence of the unlabeled capture-(miR21)-probes. The results in Figure 3D illustrate that the PCI technique can be used as a novel tool to detect miR-21 molecules for medical applications. In the presence of 100 nM miR-21 targets (Fig. 3d, lower spectrum), the SERS intensity was significantly reduced, indicating that interference of the plasmonic coupling effect was produced. However, in the absence of the target microRNA sample (Fig. 3d, upper spectrum: positive control) or in the presence of 100 nM non-complementary DNA samples (middle spectrum: negative control), the SERS signals were enhanced in both cases indicating that the plasmonic coupling effect was induced through the aggregated nanoparticles.

4) SERS Nanoprobes for Chemical Sensing

Combining the intrinsically narrow Raman peaks, which serve as spectral fingerprints, and the plasmonic effect for signal intensity enhancement, the SERS technique provides important tools for trace analysis and chemical sensing. A wide variety of metallic nanoparticles and nanoplatforms having various shapes and structures have been investigated theoretically and found to exhibit unique plasmonics properties [21, 36, 52-55]. Improved knowledge of the plasmonics effect and advances in theoretical calculation and simulation studies of the electromagnetic enhancements will lead to the design and fabrication of plasmonics-active nanostructures with optimal enhancement properties. Our laboratory has recently introduced gold nanostars as novel multi-functional plasmonic-active nanoplatforms for both sensing and therapy [40]. Gold nanostars exhibit a unique star shape and several interesting photonic properties that can be exploited for molecular imaging and cancer therapy. In contrast to other nanoparticles that requires hours of elaborate chemical processes, our high-yield nanostar synthesis method is simple and takes less than 30 seconds to complete. Unlike most nanoparticle synthesis methods that use cetyltrimethylammonium bromide (CTAB) or poly N-vinylpyrrolidone (PVP), our synthesis method requires no addition of surfactant, rendering the surfactant-free nanostar biocompatible and surface functionalizable (Figure 4, Top). These features are important for biomedical applications. The optical properties of nanostars having different branches (S10–S30) were calculated [48]. The 3D nanostar simulations were performed using the finite-element method (FEM)-based software package Comsol Multiphysics v3.4, which yields solutions to the local E-field around 3D metallic nanostructures. The scattering and absorption behavior of our nanostars was investigated by evaluating the polarization-averaged scattered E-fields in their vicinity as they were discretely rotated around the x-y axis in 3D space. Figure 4 (Bottom) depicts that the local E-field is most greatly enhanced at the tips of those branches that are aligned, at least partially, with the incident polarization. The enhancement was strongest when the particle's plasmon resonance matched the incident energy. To date, implementing gold nanoparticles for biomedical applications has generated strong interest. In particular, two major potential applications utilizing two-photon photoluminescence imaging and photothermal cancer therapy will be highlighted.

In general, metal nanoparticles tend to aggregate in solution, thus preventing quantitative analysis. However, when they are coated with surfactants or organic ligands such as PEG, or inorganic materials such as silica, nanoparticles remain non-aggregated and allow quantitative analysis. A method The development of gold nanoparticles coated with ultrathin

Author Manuscript Author Manuscript Author Manuscript Author Manuscript

silica shells has led to a method by which SERS can be obtained from virtually any surface. [76, 77] Figure 5 illustrates the possibility of using NIR dye-labeled gold nanostars for SERS quantitative analysis. Using a 785-nm laser at 230 mW, the SERS spectra were measured using DTTC (an NIR dye) embedded in silica-coated gold nanostars over a range of concentrations from 0 to 0.125 nM showing a linear and reproducible response.

The exquisite spectral specificity of SERS in chemical sensing is illustrated in our studies related to pH sensing. Local pH environment is an important physiological biomarker for tumor detection since solid tumors contain a highly acidic internal environment due to high glucose metabolism rate and poor perfusion. Furthermore, knowledge of intracellular pH values is essential in cellular studies of protein structure, enzymatic catalysis, drug delivery and effects of cellular transport and exposure to environmental toxicants. Fluorescence has been used for pH detection but suffers from tissue autofluorescence background and photobleaching. A plasmonics-active nanosensor has been developed for intracellular measurement of pH in single living human cells using SERS detection [56]. The nanoprobe is functionalized with thiolated ligands or labels, thereby imparting the molecular specificity required for intracellular biodetection and bioanalysis. The fabrication of the pH nanosensor is similar to that of previous nanosensors developed for single-cell analysis [57-60] by tapering optical fibers using a commercially available pipette puller, producing nanoprobes of 30-50 nm in diameter. These nanobiosensors combining molecular bio-recognition with nanotechnology provide powerful new techniques for *in vivo* monitoring of biochemical processes in a living cell [60]. Antibody-based nanosensors were developed to monitor the carcinogen benzo[a]pyrene (BaP) [57], benzopyrene tetrol (BPT), a DNA-adduct biomarker of human exposure to the BaP [58], and apoptosis in a single cell following photodynamic therapy [59]. For measuring pH, these tapered optical fibers were coated with a 6-nm mass thickness of silver at ~ 10^{-7} torr atmospheric pressure using an electron beam evaporator. Following Ag island film (AgIF) deposition, the nanoprobes were functionalized for 15 seconds in 10 mM paramercaptobenzoic acid (pMBA) dissolved in ethanol, which anchored pMBA to the AgIF via a silver-thiol covalent bond. The carboxyl group of pMBA is pH sensitive across the physically relevant range, thereby rendering the nanoprobe pH sensitive across that range as well. The effectiveness and usefulness of the SERS nanoprobes are illustrated by measurements of pH values inside HMEC-15/hTERT immortalized “normal” human mammary epithelial cells and PC-3 human prostate cancer cells [56].

Plasmonic gold nanostars have been developed for pH sensing in a study combining theoretical and experimental investigations [61]. SERS spectral changes of the pH-sensitive dye (pMBA) in the range 1000-1800 cm^{-1} with pH variation between 5 and 9 were identified in experiments (Figure 6) and vibrational modes were assigned using theoretical calculations. In order to investigate those SERS spectrum changes observed in the experiments, Density Functional Theory (DFT) calculations were performed for simulation models of pMBA-Au and pMBA-Ag (Fig. 6A) since the synthesized nanostar has been reported to contain a major percentage of gold and a minor percentage of silver. All quantum chemical calculations were performed with the program package Gaussian 03. DFT calculations with the B3LYP functional and 6-311++G (d, p) basis set were used for all the atoms except gold or silver in the optimization of the ground state geometries and

Author Manuscript Author Manuscript Author Manuscript Author Manuscript

simulation of the vibrational spectra. The Raman peaks of pMBA at protonated and deprotonated states from DFT calculations are shown in Fig. 6B. The Raman peak position for benzene ring stretching at ~1580 cm^{-1} (Fig 6C) was identified to be a unique index for pH sensing since it was found to have a consistent downshift when pH value increases (Fig. 6D). The calculated Raman peak for this vibrational mode has a 26.2 cm^{-1} down-shift when the simulated pMBAAu complex changes from the protonated to deprotonated state. This phenomenon is confirmed and well-explained with DFT simulation to be due to the coupling between the benzene ring stretching mode and the carboxylic group stretching mode. This unique pH sensing index could be used for chemical sensing and molecular imaging applications. The use of nanosensors and nanoprobes could provide unprecedented insights into intact cell function, allowing studies of molecular functions in the context of the functional cell architecture in an integrated system approach.

5) Two-Photon Luminescence and Photothermal Nanotherapy Using Plasmonic Gold Nanostars *Two-photon photoluminescence imaging*

Two-photon photoluminescence (TPL) imaging offers a strong optical contrast mechanism for viewing metal nanoparticles in real-time [78, 48]. Traditionally, detection of metal nanoparticles requires the use of transmission electron microscopy or inductively-coupled plasma mass spectroscopy, both of which are not suitable for imaging live specimens. Dark-field microscopy or reflectance confocal microscopy have been applied but are limited by poor imaging resolution especially in tissue samples. Under single-photon excitation, gold nanoparticles exhibit extremely weak luminescence. The development of multiphoton microscopy, which is based on femtosecond pulsed laser excitation, offers a new way to visualize single metal nanoparticle with superior resolution [79]. Interestingly, multiphoton-induced photoluminescence intensity changes dramatically in regard to the localized surface plasmon resonance. The visible photoluminescence is attributed to interband recombination of holes in the *d* band with electrons in the conduction band near the Fermi surface [80]. By tuning the surface plasmon of metal nanoparticles to match the multiphoton laser excitation wavelength, high-resolution imaging of gold nanoparticles has been reported in several studies [78, 48, 81-85], including assessing the intracellular distribution and quantity of nanoparticles (NPs) [40, 41, 45, 86-91], to visualize membrane receptors [92], and to detect cancer cells [48, 82, 84, 87, 93, 94].

Plasmonic gold nanostars have recently been applied for TPL imaging by Wei *et al.* and Yuan *et al.*, who first reported nanostars' TPL imaging *in vitro* and *in vivo*, respectively [48, 91]. A quadratic dependence of TPL intensity on nanostars (excitation power below 10 mW) indicated an underlying nonlinear two-photon process on nanostars [48]. The TPL excitation matches the nanostars' plasmon spectra, indicating an underlying TPL mechanism involving plasmon coupling [95]. In contrast to other NIR-plasmonic nanoparticles, nanostars not only have plasmon in the NIR range but also multiple sharp tips creating a "lightning rod" effect that further enhances the local surface plasmons.

The combined effect from these two properties leads to a two-photon action cross section (TPACS) of nanostars up to 10^{6-7} Göeppert-Mayer units (GM) 648], which is higher than that of quantum dots (10^4-10^5 GM) and organic fluorophores (10^2-10^3 GM). With such a

Author Manuscript Author Manuscript Author Manuscript Author Manuscript

high TPACS, nanostars have been used to study nanoparticle uptake profiles *in vitro* and the real-time tracking of nanostars *in vivo* [40, 41, 48]. To enhance cellular uptake TAT-NS were synthesized as illustrated in Figure 7A (41). The TAT nuclear targeting peptide, an HIV-1 protein-derived TAT sequence, has been previously shown to aid entry of cargo through the cell membrane via normal cellular processes and, furthermore, to localize small cargo to the nucleus of the cell. Silver nanoparticles co-functionalized with the TAT peptide showed greatly enhanced cellular uptake over the control nanoparticles lacking the targeting moiety [37]. TAT-peptide functionalized gold nanostars (NS) are taken up by cells significantly more readily than bare or PEGylated NS (Figure 7B). The cellular uptake mechanism involves actin-driven lipid raft-mediated macropinocytosis, where particles primarily accumulate in macropinosomes but may also leak out into the cytoplasm [41].

Photothermal Nanotherapy

Photothermal therapy involves treating cancer through hyperthermia generated by photon energy. Since cancer cells are more susceptible to elevated temperature (> 42 °C) than normal cells, hyperthermia has been used to treat cancer for many years [96, 97]. Conventionally, hyperthermia is delivered using microwaves or heat applicators. However, these methods are not suitable for deep-seated tumor and the heating distribution is often not well controlled. Another therapeutic modality, high-intensity focused ultrasound (HIFU) has been used for selective heating of deep tumor, but it typically requires a clear acoustic window and relatively long treatment duration. More importantly, these methods are only macroscopically confined to the tumor area but are not tumor-specific at the cellular level. To improve tumor specificity and efficacy, the therapeutic agent needs to go inside the tumor, be retained in the tumor, and then transduce external stimuli to activate the therapeutic process. Such a strategy is the fundamental approach of our group for photothermal cancer therapy using nanoparticles, which we referred to here as photothermal nanotherapy. Following intra-tumoral delivery, the nanoparticle acts as a photothermal transducer to efficiently convert photon energy to heat for selective cancer therapy at the nanoscale level with the use of nanoparticles. In particular, NIR-plasmonic gold nanoparticles have become one of the most efficient photothermal transducers that operates in the tissue optic window for deep tissue heating. A NIR-plasmonic gold nanoparticle exhibits a high absorption-to-scattering ratio (> 9) and extinction coefficient (up to 10^{10} M^{-1} cm^{-1}), which is much greater than that of QDs (10^{4} M^{-1} cm^{-1}), fluorescein (10^{5} M^{-1} cm^{-1}) and carbon nanotubes ($10^{4\text{-}5}$ M^{-1} cm^{-1}), making gold nanoparticles a powerful photothermal therapeutic agent [40, 98]. Various photothermal therapy studies using plasmon-enhanced local tumor hyperthermia have been demonstrated [99, 100].

We have demonstrated that NIR-plasmonic gold nanostars provide an effective platform for photothermal therapy. Fabricated using a simple surfactant-free plasmon-tunable synthesis method [48], nanostars exhibit a high absorption-to-scattering cross section ratio due to the presence of multiple thin branches on a small core [40]. Multiple sharp branches are also more favorable for heat generation than single branch or spherical nanoparticles. Lu *et al.* and Yuan *et al.* applied star-shaped nanoparticles to photothermal therapy for the first time *in vitro* and *in vivo*, respectively [101, 40]. Using the TAT peptide-functionalized nanostars to facilitate the intracellular delivery followed by irradiation with a femto-second pulsed

Author Manuscript Author Manuscript Author Manuscript Author Manuscript

laser, a successful *in vivo* photothermal therapy was achieved under an irradiance of 0.2 W/cm [41], which is below the maximal permissible exposure of skin per ANSI regulation (Figure 8). These studies demonstrated that gold nanostars have great potential for use in photothermal cancer nanotherapy.

7) Theranostics Combining SERS Detection and Photodynamic Therapy

While the early applications of SERS focused mainly on spectrochemical analyses, there have been a growing number of reports using Raman dye-labeled nanoparticles as SERS tags in recent years. These tags provide numerous advantages over the conventional fluorophore in labeling applications. SERS tags are well suited for multiplex detection with the narrow, fingerprint-like Raman spectra and need for only one excitation source, whereas fluorophores typically have very broad, featureless emission peaks that require a specific wavelength for excitation. Another advantage is that SERS tags do not suffer from photobleaching and matrix effects that are often troublesome for fluorescence-based assays. Nanoparticle-based labels are also more robust than free dye molecules as they can be encapsulated in an inert shell, such as silica, to prevent degradation in biological environments.

The gold nanostar platform that was recently developed in our laboratory has proven to be an excellent substrate for creating SERS tags [39, 43, 45, 46]. The multiple branches of the nanostars' geometry produce strong enhancement of the EM field due to the 'lightning rod' effect [48]. Since the base of the adjacent branches in the nanostars act as 'hot spots' on each particle, aggregation is not required to obtain SERS, whereas with spherical particles aggregation is required to create hot spots. It is possible to control the synthesis of nanostars such that their surface plasmon resonance (and maximum EM enhancement) are tuned in the NIR spectral range of the tissue diagnostics window (700-1200nm), an advantage for biological applications. When encapsulated in a silica shell, Raman-labeled nanostars become capable of both carrying drugs within the porous silica matrix and serving as an imaging agent. We have demonstrated this theranostic capability (therapy and diagnostics) by loading photosensitizing drugs onto the particles for photodynamic therapy (PDT), a promising modality for the treatment of a variety of diseases. Following activation by light at the appropriate wavelength, the photosensitizer molecule is excited to a singlet state, and then to the triplet state via spin-orbit coupling, followed by energy transfer to nearby oxygen molecules, which results in the production of reactive oxygen species (ROS). These ROS species can then damage nearby cellular components and cause cell death by apoptosis or necrosis [102].

The combination of SERS tag and PDT drug carrier into a single platform is promising for theranostic applications. Our first proof-of-concept design used a NIR Raman dye labeled nanostar with the photosensitizer methylene blue (MB) encapsulated in a silica shell around the particles [39]. Figure 9A provides a schematic overview of this design. The gold nanostars were first labeled with a NIR Raman dye, and then coated with silica that was embedded with MB. Excitation at 785 nm produces a strong SERS signal from the Raman dye on the nanostar core. This wavelength of light also falls outside of the absorption band of MB, thus preventing any unwanted activation of the photosensitizer. When exposed to

Author Manuscript Author Manuscript Author Manuscript Author Manuscript

633-nm light, fluorescence (and singlet oxygen) from the embedded MB is observed. As can be seen in Figure 9B, cell death only occurs in the area that was irradiated. Figure 9C shows that when nanostars are coated with silica without embedded MB, 633-nm laser exposure has no effect on the cells.

After demonstrating the feasibility of using such a nanoconstruct for both detection and treatment, we applied the platform to intracellular Raman imaging and photodynamic therapy *in vitro* (Figure 10) [46]. The theranostic nanoplatform was further functionalized with a cell-penetrating peptide, TAT, which increased the efficacy of our construct by increasing intracellular accumulation of particles [37]. In this case, the particles were labeled with a dye to match the 633-nm laser excitation of our Raman mapping system. Protoporphyrin IX was encapsulated in the silica shell as the PDT drug, and was activated using UV light from a filtered mercury lamp. Figure 10D shows a dramatic increase in intracellular particle accumulation when the particles were functionalized with the TAT peptide, after a 1 hour incubation period with the cells. The greater number of particles per cell allows for effective Raman imaging (Figure 10E) and PDT (Figure 10F) with the short incubation time used. In contrast, without TAT, there are not enough particles within the cells to allow Raman imaging (Figure 10B) or to be effective for PDT (Figure 10C). Results of the live/dead staining are shown in Figs. 10C and 10D. Live cells are stained green and dead cells are stained red. Cell death due to PDT is highly evident in Fig. 10D. These results show the potential for using SERS-labeled nanoplatforms for both detection and treatment of disease.

8. Conclusion

Plasmonics-active nanoplatforms offer a number of important advantages in chemical sensing, imaging and medical diagnostics. The Molecular Sentinel nanoprobe technique can provide a useful tool for multiplexed DNA detection in a homogeneous solution for medical diagnostics and high throughput bioassays. The results demonstrate the specificity and selectivity of the MS nanoprobes, as well as the ability to use multiple MS nanoprobes for multiplexed DNA detection. The ability to simultaneously detect multiple nucleic acid biomarkers (such as DNA, mRNA, miRNA) is critical for many applications such as high-throughput screening and systems biology research and early medical diagnostics at the gene and molecular level. In particular, the development of practical and sensitive detection techniques with highly multiplexing capability, such as SERS-based techniques, could lead to personal medicine and improved accuracy for disease diagnosis, since a variety of molecular alterations in multiple genes are usually involved in progression of various illnesses ranging from cancers to infectious diseases. The MS sensing scheme can be adapted readily to a chip platform, such the Nanowave chip, the fabrication of which is simple and low in cost with high reproducibility. Furthermore, the SERS measurements can be performed immediately following the hybridization reactions involving a homogeneous assay without washing steps, which greatly simplifies the assay procedures.

Plasmonics–active probes such as gold nanostars provide an excellent theranostic platform, combining two-photon luminescence with photothermal therapy or Raman imaging and photodynamic therapy. The use of the cell-penetrating peptide, TAT, greatly increases

Author Manuscript Author Manuscript Author Manuscript Author Manuscript

particle uptake by the cells, enhancing the efficacy of the nanostars construct. The particles exhibited no cytotoxic effect under dark conditions. The results of animal experiments indicate that the nanostars provide a useful nanoplatform for *in vivo* sensing and therapeutic applications. Due to the well-established strengths of SERS including a lack of photobleaching and photodegradation, the ability to perform multiplexed bioanalysis using a single laser wavelength, and narrow spectral width of Raman bands, the multiplexing capability of Raman and SERS techniques is excellent in comparison to the other spectroscopic alternatives, thus for many applications in *in vitro* and *in vivo* medical diagnostics, environmental exposure assessment, drug development and high throughput screening. The combination of plasmonics-enhanced SERS sensing and treatment (e.g., photothermal and photodynamic modalities) will opening new horizons to future theranostic applications.

ACKNOWLEDGMENTS

This work was sponsored by the National Institutes of Health (Grant RO1 341 EB006201), the Department of Defense (DOD Award W81XWH-09-1-0064), and the Defense Advanced Research Projects Agency (HR0011-13-2-0003). The content of the information does not necessarily reflect the position or the policy of the Government, and no official endorsement should be inferred.

REFERENCES

1. Jeanmaire DL, Van Duyne RP. J. Electroanal. Chem. 1977; 84:1–20.
2. Albrecht MG, Creighton JA. J. Am. Chem. Soc. 1977; 99:5215–5217.
3. Moskovits M. Rev. Mod. Phys. 1985; 57:783–826.
4. Wokaun A, Gordon JP, Liao PF. Phys. Rev. Lett. 1982; 48:957–960.
5. Schatz GC. Acc. Chem. Res. 1984; 17:370–376.
6. Kerker M. Acc. Chem. Res. 1984; 17:271–277.
7. Chang, RK.; Furtak, TE. Surface-Enhanced Raman Scattering. Plenum Press; 1982.
8. Pockrand, I. Surface-Enhanced Raman Vibrational Studies at Solid/Gas Interfaces. Springer; 1984.
9. Vo-Dinh T, Hiromoto MYK, Begun GM, Moody RL. Anal. Chem. 1984; 56:1667–1670.
10. Meier M, Wokaun A, Vo-Dinh T. J. Phys. Chem. 1985; 89:1843–1846.
11. Vo-Dinh T, Meier M, Wokaun A. Anal. Chim. Acta. 1986; 181:139–148.
12. Enlow PD, Buncick M, Warmack RJ, Vo-Dinh T. Anal. Chem. 1986; 58:1719–1724.
13. Vo-Dinh T, Uziel M, Morrison A. Appl. Spectrosc. 1987; 41:605–610.
14. Moody RL, Vo-Dinh T, Fletcher WH. Appl. Spectrosc. 1987; 41:966–970.
15. M Alak A, Vo-Dinh T. Anal. Chem. 1987; 59:2149–2153. [PubMed: 3674432]
16. Alak AM, Vo-Dinh T. Anal. Chim. Acta. 1988; 206:333.
17. Vo-Dinh T, Alak A, Moody RL. Spectrochim. Acta B. 1988; 415:605–615.
18. Bello JM, Stokes DL, Vo-Dinh T. Anal. Chem. 1989; 61:1779–1783.
19. Bello JM, Stokes DL, Vo-Dinh T. Appl. Spectrosc. 1989; 43:1325–1330.
20. Vo-Dinh T, Houck K, Stokes DL. Anal. Chem. 1994; 66:3379–3383. [PubMed: 7978314]
21. Vo-Dinh T. Trends in Anal. Chem. 1998; 17:557–570.
22. Stokes DL, Chi Z, Vo-Dinh T. Appl. Spectrosc. 2004; 58:292–298. [PubMed: 15035709]
23. Isola NR, Stokes DL, Vo-Dinh T. Anal. Chem. 1998; 70:1352–1356. [PubMed: 9553492]
24. Zeisel D, Deckert V, Zenobi R, Vo-Dinh T. Chem. Phys. Lett. 1998; 283:381–385.
25. Khoury C, Vo-Dinh T. J. Phys. Chem. C. 2008; 112:18849–18859.
26. Scaffidi J, Gregas M, Vo-Dinh T. Anal. Bioanal. Chem. 2009; 393:1135–1141. [PubMed: 19066865]

Author Manuscript Author Manuscript Author Manuscript Author Manuscript

27. Vo-Dinh T, Allain LR, Stokes DL. J. Raman Spectrosc. 2002; 33:511–516.
28. Vo-Dinh T, Yan F, Wabuyele M. J. Raman Spectrosc. 2005; 36:640–647.
29. Wabuyele M, Yan F, Griffin G, Vo-Dinh T. Rev. Scientif. Instrum. 2005; 76:063710, 1–7.
30. Wabuyele M, Vo-Dinh T. Anal. Chem. 2005; 77:7810–7815. [PubMed: 16316192]
31. Chen K, Leona M, Vo-Dinh KC, Yan F, Wabuyele MB, Vo-Dinh T. J. Raman Spectrosc. 2005; 37:520–527.
32. Vo-Dinh T. IEEE J. Selected Topics in Quantum Electronics. 2008; 14:198–205.
33. Wang HN, Vo-Dinh T. Nanotechnology. 2009; 20:065101, 1–6. [PubMed: 19417369]
34. Wabuyele MB, Yan F, Vo-Dinh T. Anal. Bioanal. Chem. 2010; 398:729–736. [PubMed: 20676618]
35. Vo-Dinh T, Wang HN, Scaffidi J. J. Biophotonics. 2010; 3:89–102. [PubMed: 19517422]
36. Vo-Dinh T, Dhawan A, Norton SJ, Khoury CG, Wang H-N, Misra V, Gerhold M. J. Phys. Chem. C. 2010; 114:7480–7488.
37. Gregas MK, Scaffidi JP, Lauly B, Vo-Dinh T. Applied Spectrosc. 2010; 64:858–866.
38. Gregas MK, Scaffidi JP, Lauly B, Vo-Dinh T. Nanomedicine. 2011; 7:115–122. [PubMed: 20817123]
39. Fales AM, Yuan H, Vo-Dinh T. Langmuir. 2011; 27:12186–12190. [PubMed: 21859159]
40. Yuan H, Khoury CG, Wilson CM, Grant GA, Bennett AJ, Vo-Dinh T. Nanomedicine: NBM. 2012; 8:1355–1363.
41. Yuan H, Fales AM, Vo-Dinh T. J. Am. Chem. Soc. 2012; 134:11358–11361. [PubMed: 22734608]
42. Khoury C, Vo-Dinh T. J. Phys. Chem. C. 2012; 116:7534–7545.
43. Yuan H, Liu Y, Fales AM, Li YL, Liu J, Vo-Dinh T. Anal. Chem. 2013; 85:208–212. [PubMed: 23194068]
44. Wang HN, Dhawan A, Du Y, Batchelor D, Leonard DN, Misra V, Vo-Dinh T. Phys. Chem. Chem. Phys. 2013; 15:6008–6015. [PubMed: 23493773]
45. Yuan HK, Fales AM, Khoury CG, Liu J, Vo-Dinh T. J. Raman Spectrosc. 2013; 44:234–239. [PubMed: 24839346]
46. Fales A, Yuan H, Vo-Dinh T. Mol. Pharmaceut. 2013; 10:2291–2298.
47. Wang HN, Vo-Dinh T. Small. 2011; 7:3067–3074. [PubMed: 21913327]
48. Yuan H, Khoury CG, wang HH, Wilson CM, Grant GA, Vo-Dinh T. Nanotechnology. 2012; 23:075102, 1–9. [PubMed: 22260928]
49. Wang HN, Fales AM, Zaas AK, Woods CW, Burke T, Ginsburg G, Vo-Dinh T. Anal. Chim. Acta. 2013; 5:153–158. [PubMed: 23790305]
50. Ngo HT, Wang HN, Fales AM, Vo-Dinh T. Anal. Chem. 2013; 85:6378–6383. [PubMed: 23718777]
51. Yuan H, Register JK, Wang HN, Fales AM, Liu Y, Vo-Dinh T. Anal. Bioanal. Chem. 2013 in press. DOI 10.1007/s00216-013-6975.
52. Norton SJ, Vo-Dinh T. IEEE Trans. Nanotechnology. 2007; 6:627–638.
53. Norton SJ, Vo-Dinh T. J. Opt. Soc. Amer. 2008; 25:2767–2775.
54. Dhawan A, Gerhold M, Madison A, Fowlkes J, Russell P, Vo-Dinh T, Leonard D. Scanning. 2009; 31:139–146. [PubMed: 19670460]
55. Dhawan A, Du Y, Batchelor Y,D, Wang H-N, Hsin-Neng, Leonard D, Misra V, Veena, Ozturk M, Gerhold M, Vo-Dinh T. Small. 2011; 7:727–731. [PubMed: 21425456]
56. Scaffidi JP, Gregas MK, Seewaldt V, Vo-Dinh T. Anal. Bioanal. Chem. 2009; 393:1135–1141. [PubMed: 19066865]
57. Vo-Dinh T, Alarie JP, Cullum B, Griffin GD. Nature Biotechnology. 2000; 18:764–767.
58. Cullum B, Griffin GD, Miller GH, Vo-Dinh T. Anal. Biochem. 2000; 277:25. [PubMed: 10610686]
59. Kasili PM, Song JM, Vo-Dinh T. J. Am. Chem. Soc. 2004; 126:2799–2806. [PubMed: 14995197]
60. Vo-Dinh T, Kasili PM, Wabuyele MB. Nanomedicine. 2006; 2:22–30. [PubMed: 17292112]
61. Liu Y, Yuan H, Fales AM, Vo-Dinh T. J. Raman Spectrosc. 2013 DOI: 10.1002/jrs.4302.

Author Manuscript Author Manuscript Author Manuscript Author Manuscript

62. Kneipp K, Wang Y, Kneipp H, Perelman LT, Itzkan I, Dasari R, Feld MS. Phys. Rev. Lett. 1997; 78:1667–1670.
63. Nie S, Emory SR. Science. 1997; 275:1102–1106. [PubMed: 9027306]
64. Michaels AM, Jiang J, Brus L. J. Phys. Chem. B. 2000; 104:11965–11971.
65. Xu H, Aizpurua J, Kaell M, Apell P. Phys. Rev. E. 2000; 62:4318–4324.
66. Graham D, Smith WE, Linacre AMT, Munro CH, Watson ND, White PC. Anal. Chem. 1997; 69:4703–4707.
67. Cao YC, Jin R, Mirkin CA. Science. 2002; 297:1536–1541. [PubMed: 12202825]
68. Huschka R, Barhoumi A, Liu Q, Roth JA, Lin Ji, Halas NJ. ACS Nano. 2012; 6:7681–7691. [PubMed: 22862291]
69. Dick LA, McFarland AD, Haynes CL, Duyne RP. J. Phys. Chem. B. 2001; 106:853–860.
70. Xu H, Aizpurua J, Käll M, Apell P. Phys. Rev. E. 2000; 62:4318–4324.
71. Lassiter JB, Sobhani H, Knight MW, Mielczarek WS, Nordlander P, Halas NJ. Nano Lett. 2012; 12:1058–1062. [PubMed: 22208801]
72. Mirkin CA, Letsinger RL, Mucic RC, Storhoff JJ. Nature. 1996; 382:607–609. [PubMed: 8757129]
73. Zanchet D, Micheel CM, Parak WJ, Gerion D, Williams SC, Alivisatos AP. J. Phys. Chem. B. 2002; 106:11758–11763.
74. Graham D, Thompson DG, Smith WE, Faulds K. Nature Nanotechnology. 2008; 3:548–551.
75. Qian X, Zhou X, Nie S. J. Am. Chem. Soc. 2008; 130:14934–14935. [PubMed: 18937463]
76. Anema JR, Li JF, Yang ZL, Ren B, Tian ZQ. Annu. Rev. Anal. Chem. 2011; 4:129–50.
77. Tittl A, Yin X, Giessen H, Tian XD, Tian ZQ, Kremers C, Chigrin DN, Na Liu. Nano Lett. 2013; 13:1816–1821. [PubMed: 23458121]
78. Wang H, Huff TB, Zweifel DA, He W, Low PS, Wei A, Cheng J-X. Proc. Natl. Acad. Sci. U. S. A. 2005; 102:15752–15756. [PubMed: 16239346]
79. Farrer R, Butterfield F, Chen V, Fourkas J. Nano Lett. 2005; 5:1139–1142. [PubMed: 15943457]
80. Beversluis M, Bouhelier A, Novotny L. Phys. Rev, B. 2003; 68:115433.
81. Mishra A, Lai GH, Schmidt NW, Sun VZ, Rodriguez AR, Tong R, Tang L, Cheng J, Deming TJ, Kamei DT, Wong GCL. Proc. Natl. Acad. Sci. U. S. A. 2011; 108:16883–16888. [PubMed: 21969533]
82. Dowling MB, Li L, Park J, Kumi G, Nan A, Ghandehari H, Fourkas JT, Deshong P. Bioconjugate Chem. 2010; 21:1968–1977.
83. Durr NJ, Larson T, Smith DK, Korgel BA, Sokolov K, Ben-Yakar A. Nano Lett. 2007; 7:941–945. [PubMed: 17335272]
84. Tozer GM, Ameer-Beg SM, Baker J, Barber PR, Hill SA, Hodgkiss RJ, Locke R, Prise VE, Wilson I, Vojnovic B. Adv, Drug Delivery Rev. 2005; 57:135–152.
85. Au L, Zhang Q, Cobley CM, Gidding M, Schwartz AG, Chen J, Xia Y. ACS Nano. 2010; 4:35–42. [PubMed: 19954236]
86. Hutter E, Boridy S, Labrecque S, Lalancette-Hébert M, Kriz J, Winnik FM, Maysinger D. ACS Nano. 2010; 4:2595–2606. [PubMed: 20329742]
87. Cho EC, Zhang Y, Cai X, Moran CM, Wang LV, Xia Y. Angew. Chem. Int. Edit. 2013; 52:1152–1155.
88. Yelin D, Oron D, Thiberge S, Moses E, Silberberg Y. Opt. Express. 2003; 11:1385–1391. [PubMed: 19466009]
89. Nagesha D, Laevsky GS, Lampton P, Banyal R, Warner C, DiMarzio C, Sridhar S. Int. J. Nanomedicine. 2007; 2:813–9. [PubMed: 18203448]
90. Huff TB, Hansen MN, Zhao Y, Cheng JX, Wei A. Langmuir. 2007; 23:1596–1599. [PubMed: 17279633]
91. Wei Q, Song H-M, Leonov AP, Hale JA, Oh D, Ong QK, Ritchie K, Wei A. J. Am. Chem. Soc. 2009; 131:9728–9734. [PubMed: 19435348]
92. Kennedy DC, Tay L-L, Lyn RK, Rouleau Y, Hulse J, Pezacki JP. ACS Nano. 2009; 3:2329–2339. [PubMed: 19702324]
93. Chen Y, Zhang Y, Liang W, Li X. Nanomedicine: NBM. 2012; 8:1267–1270.

Author Manuscript Author Manuscript Author Manuscript Author Manuscript

94. Bickford, Sun J, Fu K, Lewinski N. Nanotechnology. 2008; 19:315102–315108. [PubMed: 21828779]
95. Tong L, Wei Q, Wei A, Cheng JX. Photochem. Photobiol. 2009; 85:21–32. [PubMed: 19161395]
96. Dewhirst MW, Vujaskovic Z, Jones E, Thrall D. Int. J. Hyperthermia. 2005; 21:779–790. [PubMed: 16338861]
97. Wust P, Hildebrandt B, Sreenivasa G, Rau B, Gellermann J, Riess H, Felix R, Schlag P. Lancet Oncol. 2002; 3:487–497. [PubMed: 12147435]
98. Wang Y, Black KC, Luehmann H, Li W, Zhang Y, Cai X, Wan D, Liu SY, Li M, Kim P, Li ZY, Wang LV, Liu Y, Xia Y. ACS Nano. 2013; 7:2068–2077. [PubMed: 23383982]
99. Xia Y, Li W, Cobley CM, Chen J, Xia X, Zhang Q, Yang M, Cho EC, Brown PK. Acc. Chem. Res. 2011; 44:914–924. [PubMed: 21528889]
100. Van de Broek B, Devoogdt N, D'Hollander A, Gijs H-L, Jans K, Lagae L, Muyldermans S, Maes G, Borghs G. ACS Nano. 2011; 5:4319–4328. [PubMed: 21609027]
101. Kennedy LC, Bickford LR, Lewinski NA, Coughlin AJ, Hu Y, Day ES, West JL, Drezek RA. Small. 2011; 7:169–183. [PubMed: 21213377]
102. Choi WI, Kim JY, Kang C, Byeon CC, Kim YH, Tae G. ACS Nano. 2011; 5:1995–2003. [PubMed: 21344891]

Author Manuscript Author Manuscript Author Manuscript Author Manuscript

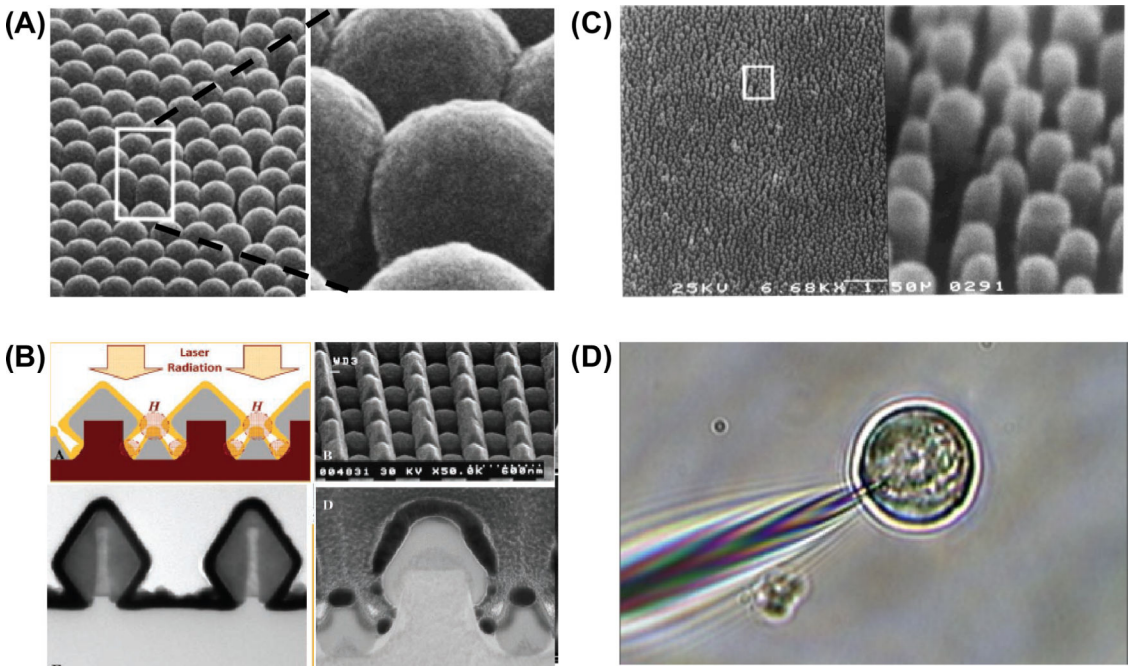

Figure 1.

SERS-active plasmonic platforms

(A) Nanowave platform consisting of nanosphere arrays coated with metal film [Adapted from Ref. 4];

(B) Top Left: Schematic of gold-coated silicon-germanium nanowires with a diamond-shaped structure, epitaxially grown from silicon nanowires; Top Right: Scanning electron microscopy (SEM) image of 2D gold-coated silicon-germanium nanowires formed on silicon-on-insulato ; Bottom Left: Transmission electron microscopy (TEM) cross-section image showing atomic layer deposition of platinum (black color) on the diamond-shaped nanowires (dark grey color) [Adapted from ref. 55]

(C)Metal film on nanorod arrays fabricated using nanolithography and plasma etching [Adapted from Ref. 12]

(D) SERS-active pH nanosensors for single-cell analysis [Adapted from Ref. 56]

Author Manuscript Author Manuscript Author Manuscript Author Manuscript

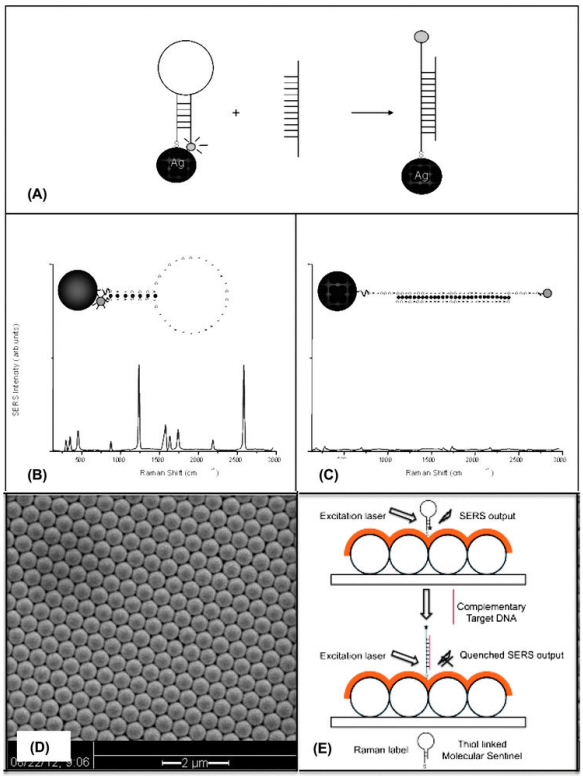

Figure 2.

(A) Operating Principle of a SERS Molecular Sentinel (MS) Nanoprobe. . *(Adapted from reference 30)*

(B) A SERS signal is observed when the MS probe is in the stem-loop conformation with the label close to the nanoparticle, inducing a strong SERS signal (closed-state),

(C) Following hybridization with a target probe, the stem opens and separates the label from the nanoparticle causing the SERS signal to decrease

(D) Application of the label-free MS detection scheme on Nanowave chip

(E) SEM image of Nanowave chip substrate. In this substrate, a monolayer of 520-nm diameter polystyrene beads is covered by a 200-nm thick Au layer. *(Adapted from reference 50)*

Author Manuscript Author Manuscript Author Manuscript Author Manuscript

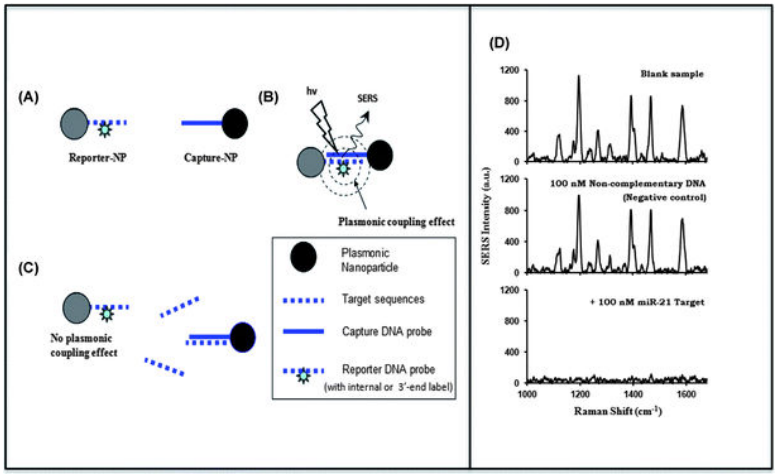

Figure 3.

The Plasmonic Coupling Interference (PCI) Detection Scheme.

(A) Silver nanoparticles are functionalized with thiolated capture oligonucleotides (Capture-NP) or complementary DNA probes labeled with a Raman dye (Reporter-NP).

(B) Plasmonic coupling effect between adjacent nanoparticles is induced by the formation of capture/reporter complementary base-paired duplexes, which couple Capture-NPs and Reporter-NPs in a short separation distance.

(C) The plasmonic coupling effect is interfered with by the formation of target/reporter duplexes.

(D) MicroRNA detection using the PCI Technique. Upper spectrum: positive control (blank) sample containing a mixture of capture-(miR21)-NPs and reporter-(miR21)-NPs. Middle spectrum: in the presence of non-complementary DNA sample as the negative control test. Lower spectrum: in the presence of complementary miR-21 targets (adapted from Ref. 47).

Author Manuscript Author Manuscript Author Manuscript Author Manuscript

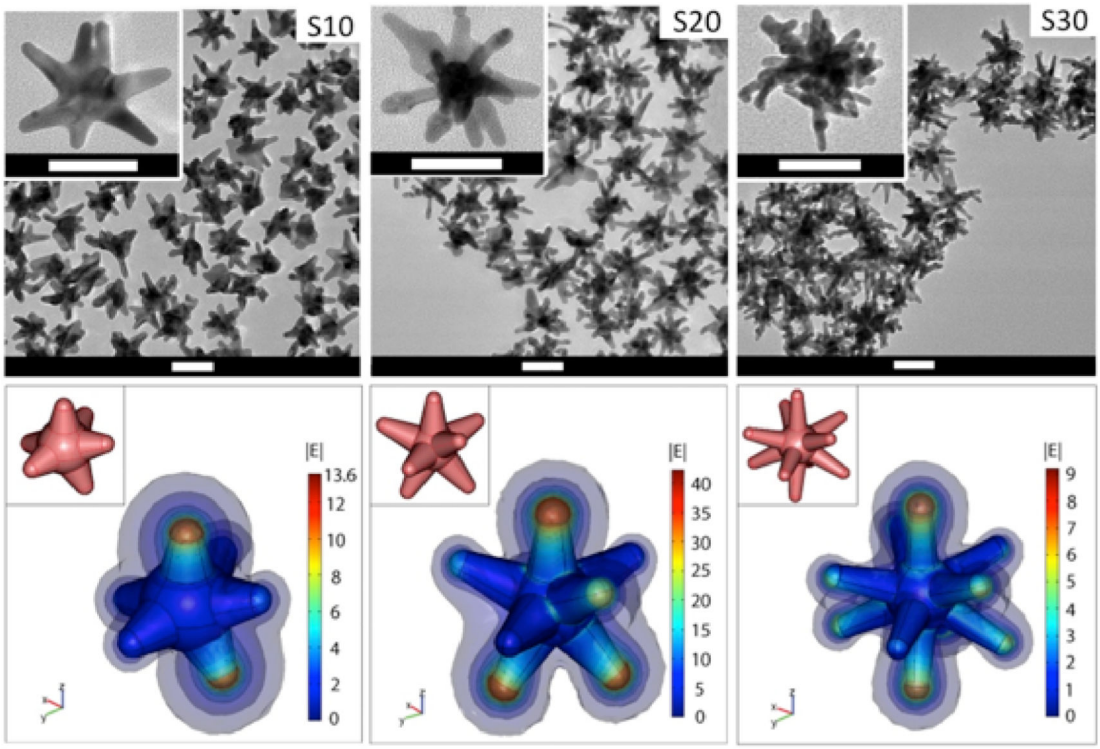

Figure 4.

(Top) TEM images of nanostars having different numbers of branches: S10 (10 branches), S20 (20 branches) and S30 (30 branches). The scale bar is 50 nm.

(Bottom) Simulation of |E| in the vicinity of the nanostars in response to a z-polarized plane wave incident E-field of unit amplitude, propagating in the y-direction, and with a wavelength of 800 nm. E-field enhancement is greatest on S20. The insets depict the 3D geometry of the stars. Diagrams are not to scale. (Adapted from Ref.48)

Author Manuscript Author Manuscript Author Manuscript Author Manuscript

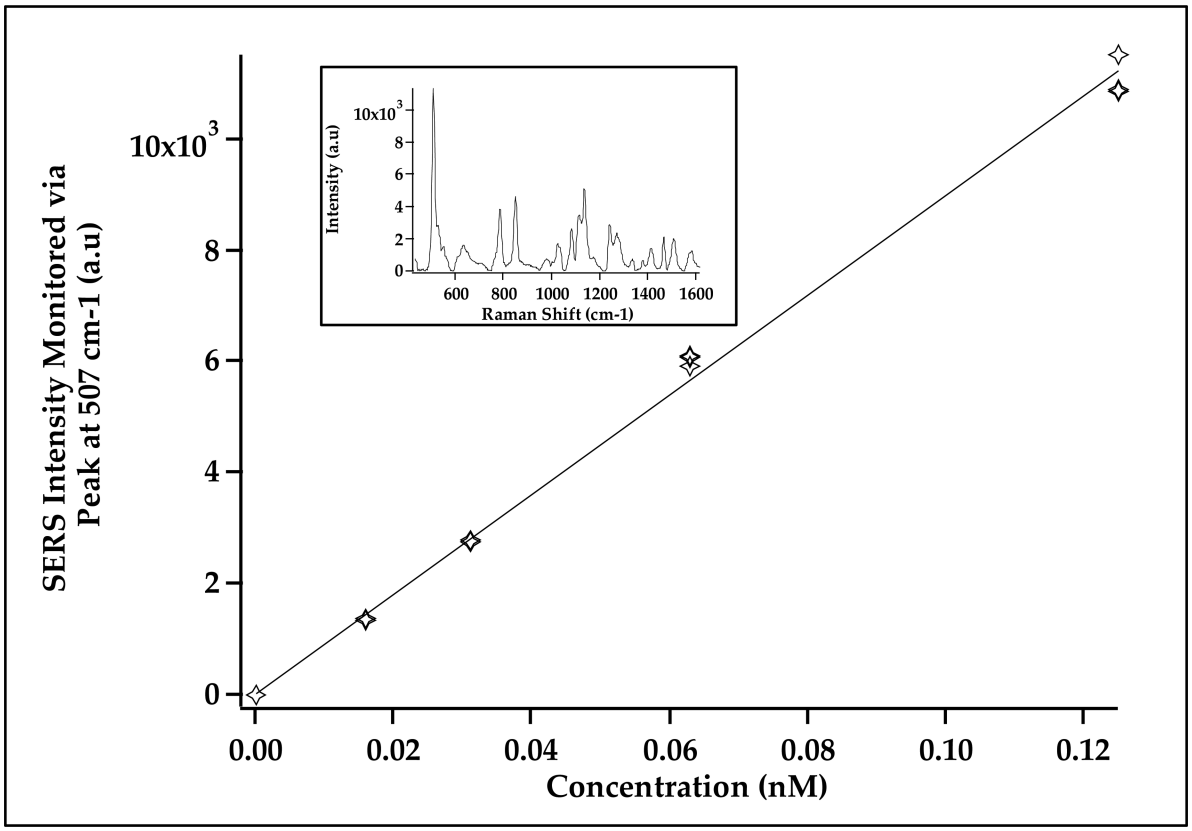

Figure 5.

Calibration curve showing SERS intensity for the NIR dye, DTTC, on gold nanostars coated with silica monitored using peak at 507 cm^{-1} over a range of concentrations from 0 to 0.125 nM. The spectra were measured using the 785-nm laser at 230 mW. Inset: Full spectrum of 0.125 nM DTTC-nanostar in solution

Author Manuscript Author Manuscript Author Manuscript Author Manuscript

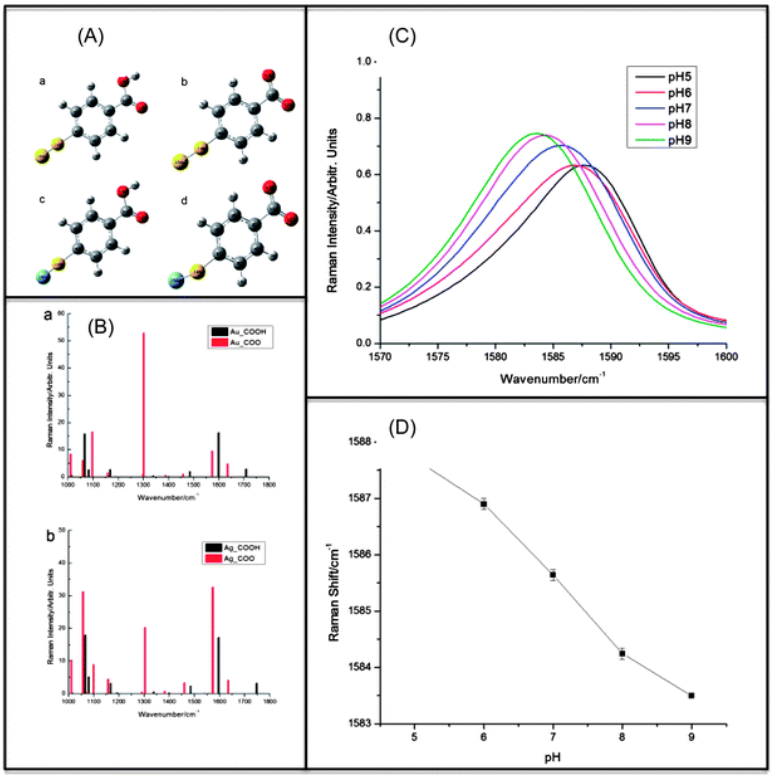

Figure 6.

SERS Nanoprobe for pH Monitoring (Adapted form Ref. 61)

(A) Molecular models for DFT calculations. a. pMBA-Au complex under the protonated state (Au_COOH). b. pMBA-Au complex under the deprotonated state (Au_COO^-). c. pMBA-Ag complex under the protonated state (Ag_COOH). d. pMBA-Ag complex under the deprotonated state (Ag_COO^-).

(B) Calculated Raman peaks for pMBA-Au and pMBA-Ag complexes at the protonated (black) and deprotonated (red) states.

(C) pH dependence of SERS spectra (1570 cm^{-1}-1600 cm^{-1}): Detail of the spectroscopic range for monitoring pH.

(D) SERS peak position as a function of pH.

Author Manuscript Author Manuscript Author Manuscript Author Manuscript

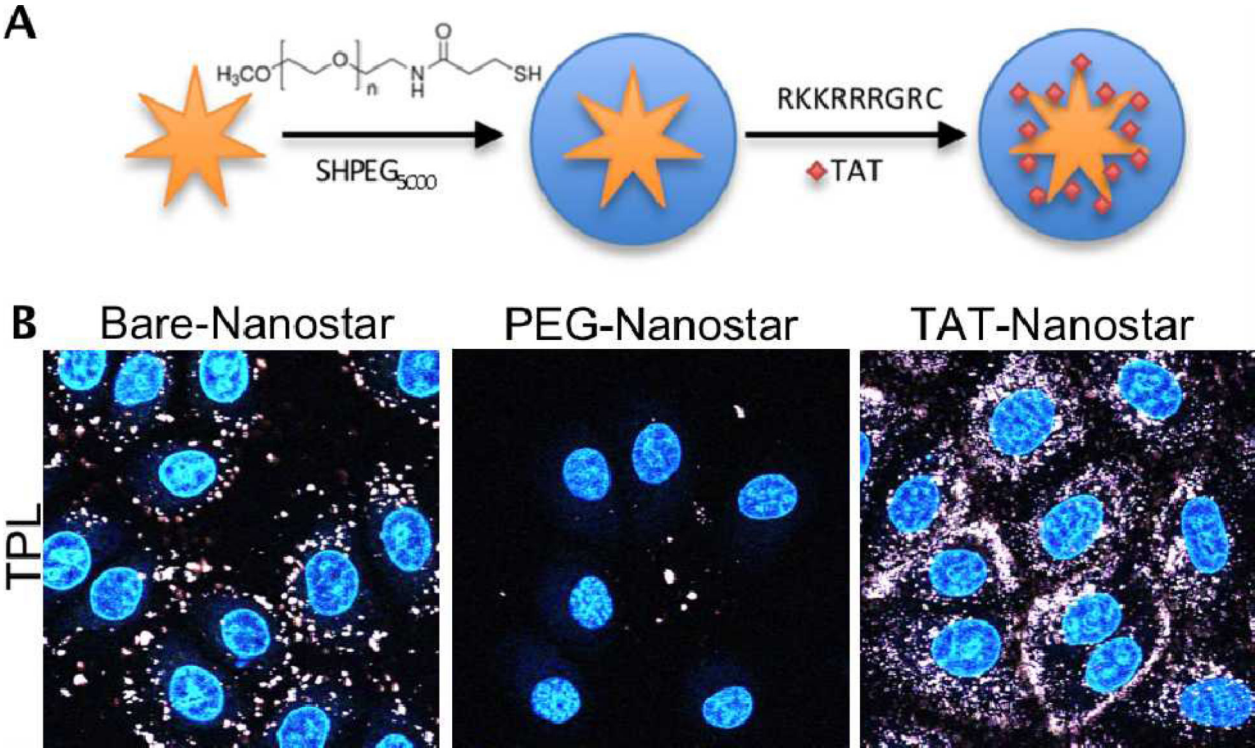

Figure 7.

TAT-functionalized gold nanostars. (A) Synthetic schematics for TAT peptide functionalization on nanostars. Bare nanostar was coated with thiolated-PEG then with cysteine-terminated TAT. (B) Cellular uptake of 0.1 nM bare nanostars, PEG-nanostars, and TAT-nanostars incubated 24 hours on BT549 cells. Aggregated bare nanostars correspond to the white big punctates on TPL image. PEG-nanostars showed very minimal uptake. Endosomal and cytosolic TAT-nanostars corresponds to the diffuse white pattern on TPL image. Nanostars are white and nuclei are stained blue. TPL image size: 125×125 μm^2. (Adapted from Ref. 41)

Author Manuscript Author Manuscript Author Manuscript Author Manuscript

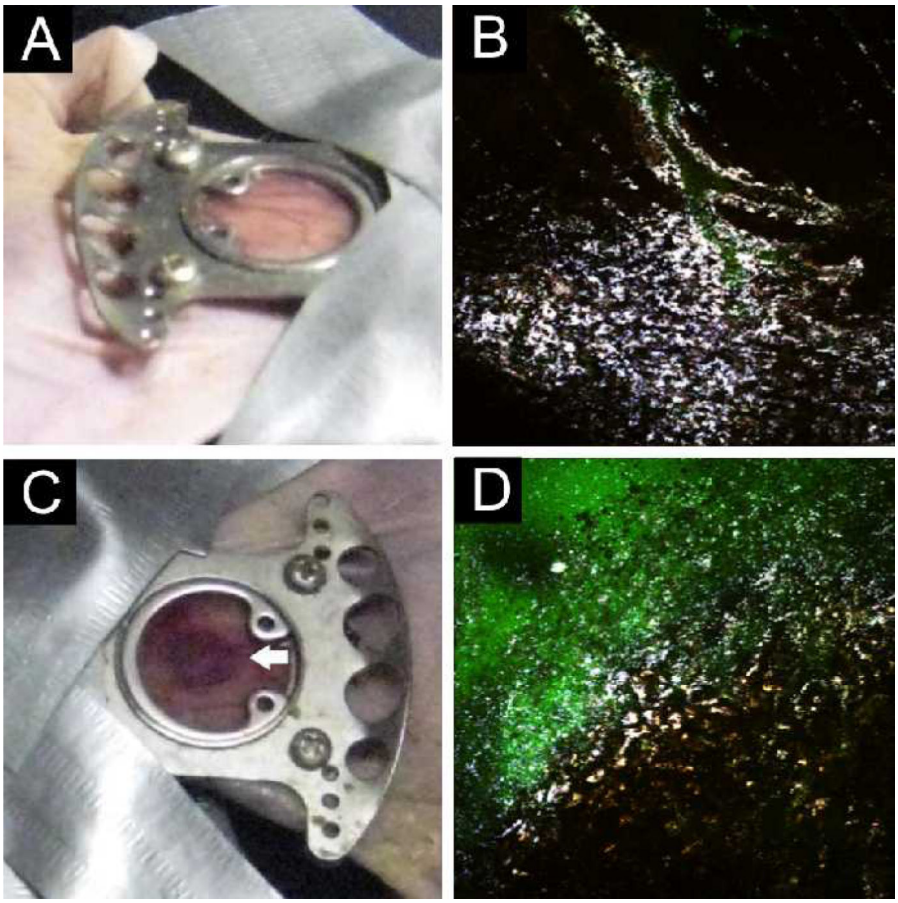

Figure 8.

Photographs and multiphoton microscopy images 48 hours after nanostars injection before (top) and after (bottom) the irradiation. (A) Before the irradiation, the window appeared intact; (B) Nanostars (white color) extravasated into the tissue and near the perivascular space; Green color from FITC-dextran delineates the blood vessels; (C) After the laser irradiation (785 nm 1.1 W/cm^2, 10 min), a localized hemorrhage was formed (white arrow); (D) Leakage of FITC-dextran into the tissue was apparent in the irradiated spot but not outside the hemorrhagic spot. Microscope images are 508×□08 μm^2. (Adapted from Ref. 40)

Author Manuscript Author Manuscript Author Manuscript Author Manuscript

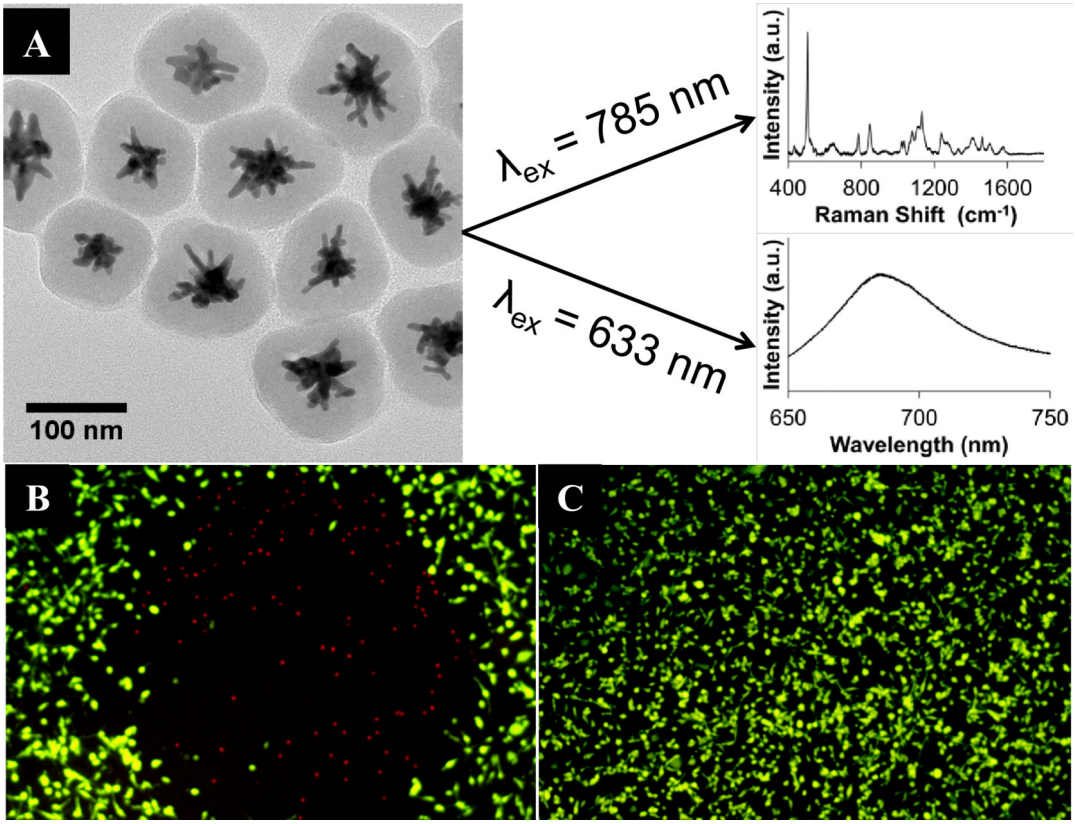

Figure 9.

(A) Overview of the proof-of-concept theranostic construct. Upon excitation at 785 nm, SERS is observed from the NIR Raman dye on the nanostar surface. Excitation at 633 nm generates fluorescence (and singlet oxygen) from the MB embedded within the silica shell. (B) shows effective PDT on breast cancer cells after incubation with MB-loaded particles and light exposure. In (C), the same light exposure was performed on cells treated with silica-coated nanostars that did not contain MB, showing no evidence of any photothermal effects. Figure adapted from [39].

Author Manuscript Author Manuscript Author Manuscript Author Manuscript

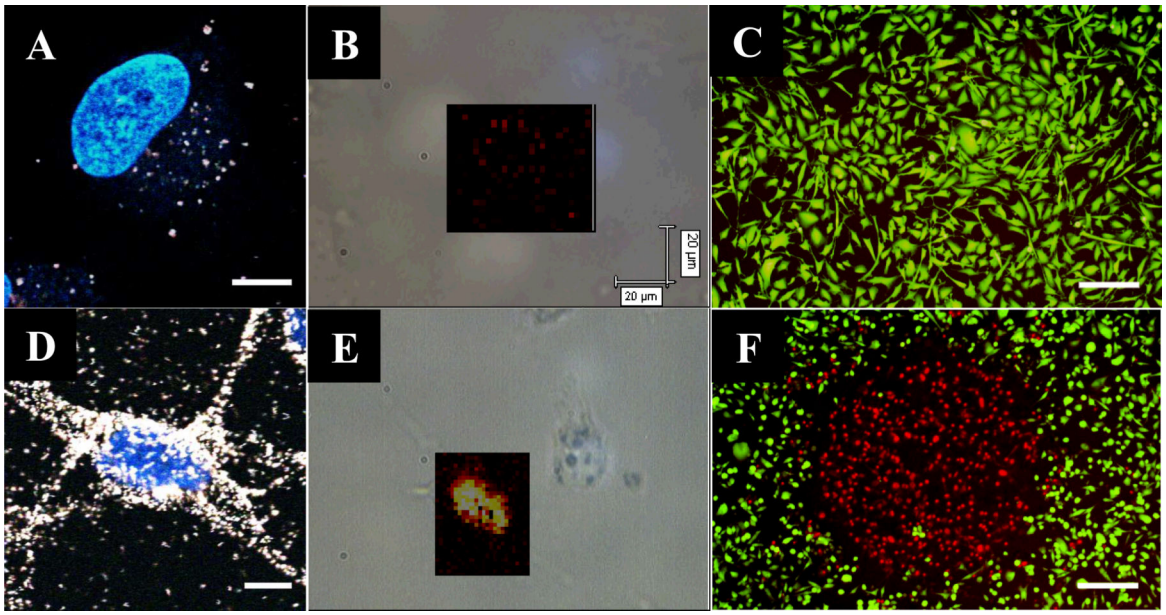

Figure 10.

Two photon luminescence imaging (A, D), Raman imaging (B, E) and cell viability after photodynamic therapy (C, F) of the theranostic nanoconstruct functionalized with (D-F) and without (A-C) the TAT peptide. Raman images were created by taking 5s acquisitions at each point (2 μm step size) over the selected area and integrating the intensity of a SERS peak from the labeled nanoparticles. For PDT, the photosensitizer was activated by exposure to UV light (30s, 4.4 W cm^{-2}). Cell viability staining was performed to visualize the effective cell destruction. Scale bars in A and D are 1 μm, the scale in B and E are the same, and the scale bars in C and F are 250 μm. Figure adapted from Ref 46.